Submillimetre-wave electron spin-resonance measurements for single-crystal $Y_2Cu_2O_5$

1996 J. Phys.: Condens. Matter 8 5461

(http://iopscience.iop.org/0953-8984/8/29/019)

J. Phys.: Condens. Matter **8** (1996) 5461–5473. Printed in the UK

Submillimetre-wave electron spin-resonance measurements for single-crystal $Y_2Cu_2O_5$

S Kimura†, H Ohta†, S Mitsudo‡, M Motokawa‡, W-J Jang§, M Hasegawa‖ and H Takei‖

† Department of Physics, Faculty of Science, Kobe University, Rokkodai 1-1, Nada-ku, Kobe 657, Japan

‡ Institute for Materials Research, Tohoku University, Katahira 2-1-1, Aoba-ku, Sendai 980-77, Japan

§ Superconductivity Research Laboratory, International Superconductivity Technology Centre, Shinonome 1-10-13, Koto-ku, Tokyo 135, Japan

‖ Institute for Solid State Physics, University of Tokyo, Roppongi 7-22-1, Minato-ku, Tokyo 106, Japan

Received 20 February 1996

Abstract. Submillimetre-wave ESR measurements for $Y_2Cu_2O_5$ single crystal have been performed for the first time in the frequency region from 60 to 383 GHz using a pulsed magnetic field up to 16 T. AFMR modes below $T_N = 13$ K have been analysed by a model proposed previously, which is essentially the molecular-field theory with the assumption of an $S = 1$ dimer of two Cu^{2+} spins. The anisotropies of the system are determined by the analysis, and they are discussed together with the results of our magnetization measurements.

1. Introduction

$Y_2Cu_2O_5$ is the impurity phase of a high-T_c superconductor $YBa_2Cu_3O_7$ and well known as the so-called blue–green phase. Initially there was no interest in this material and it was not noticed that it would show a very interesting phenomenon. Magnetic susceptibility [1] and specific heat [2] measurements for powder samples suggest that this material undergoes a long-range antiferromagnetic ordering below $T_N = 13$ K. Unlike what is found for the normal antiferromagnetic copper compounds, however, two successive metamagnetic transitions were found below T_N when an external field was applied to the *b*-axis (the easy axis) of a single crystal. Cheong *et al* [3] first observed this phenomenon, but below 5 T where the second steep magnetization change just started to appear, and their single crystal was a by-product of making a flux-grown $YBa_2Cu_3O_7$ crystal. We measured the magnetization of this material using an intentionally synthesized single crystal [4] up to 13 T—high enough to see the saturation by a pulsed field [5]—and obtained the full magnetization curve as shown in figure 1. This result is extremely unusual, because the anisotropy of Cu^{2+} spins is supposed to be smaller than the exchange interaction, and a metamagnetic transition should not occur and has never been observed in copper compounds before.

To explain this unusual behaviour of $Y_2Cu_2O_5$, we have proposed the following model, which was suggested by the fact that the magnetization curve for $\boldsymbol{H} \| b$-axis is quite similar to that of $NiCl_2 \cdot 2H_2O$ [5–7]. In $Y_2Cu_2O_5$, Cu^{2+} ions are surrounded by four oxygens forming

0953-8984/96/295461+13$19.50

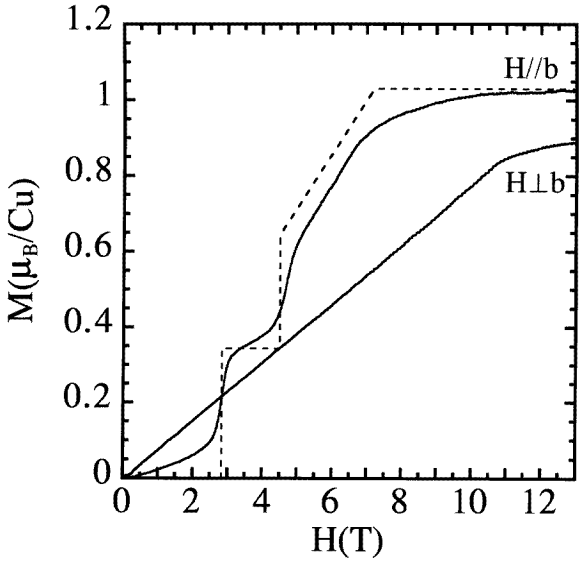

Figure 1. Magnetization curves observed in the static field at 4.2 K. The dotted line shows the calculated magnetization curve. See the text for the details.

deformed squares, and they align along the a-axis making zigzag chains [8]. It should be noticed that the 90° and the 180° exchange interaction paths are alternately connected along this chain. Neutron diffraction experiments have shown ferromagnetic arrangements of Cu^{2+} spins within the chain and along the b-axis, but an antiferromagnetic configuration between the chains in the ac-plane, below T_N at zero magnetic field [9, 10]. In our model, it is assumed that there alternately exist a strong ferromagnetic interaction J_0 and a weak interaction J_2 (ferro- or antiferromagnetic) between Cu^{2+} spins in the chain due to the 90° exchange path and the 180° one. This spin system can be regarded as a magnetic chain composed of $S = 1$ spins connected with the exchange interaction J_2 and having single-ion-type anisotropy D which is of the order of $(\Delta g/2)^2 J_0$. If D is large enough, this spin system may show metamagnetic transitions similarly to the case of $NiCl_2{\cdot}2H_2O$ [7]. This argument is our most important point. Before our model was proposed, Kazei *et al* [11] and Garcia-Munoz *et al* [12] suggested, from their powder sample magnetization measurements, that the magnetization saturated at the second metamagnetic transition field H_{c2} like the magnetization curve of $CoCl_2{\cdot}2H_2O$ [13] and did not obtain the sloping part between H_{c2} and H_s in figure 1.

From the analysis of the magnetization process using our model, the ratio of J_0 to the exchange interaction J_1 with the spins in the adjacent chain was estimated to be $|J_1/J_0| \sim 1/300$ [5, 6]. On the other hand, several models were discussed for interpreting the magnetic susceptibility of this material [14–16]. Ramakrishna and Ong reported that the magnetic susceptibility is well explained by the quasi-one-dimensional ferromagnetic chain model [14]. They analysed the experimental results assuming a uniform ferromagnetic intrachain interaction and weak antiferromagnetic interchain interactions. Janicki and Troc also analysed the magnetic susceptibility using the same model over a wide temperature range up to 1000 K [15]. Moreover Paillaud *et al* analysed the magnetic susceptibility using the J-alternating ferromagnetic chain model [16]. None of these models, however,

Table 1. The intrachain interactions J_0 and J_2, and the sums of the interchain interactions zJ_1 obtained from the magnetic susceptibility and our analysis of the AFMR. Ramakrishna and Ong, and also Janicki and Troc analysed the magnetic susceptibility assuming a uniform ferromagnetic intrachain interaction, and Paillaud *et al* assumed alternating ferromagnetic intrachain interactions. The definition of the Hamiltonian of the exchange interaction is $H = -2J \sum \boldsymbol{S}_i \cdot \boldsymbol{S}_j$

	J_0	J_2	zJ_1
Ramakrishna and Ong	36 K	36 K	−3.2 K
Janicki and Troc	88 K	88 K	−1.6 K
Paillaud *et al*	100 K	82 K	−12.4 K
Our analysis	340 K	−0.33 K	−3.68 K

can explain the metamagnetic transition of this material. The intrachain interactions J_0 and J_2 and the sums of the interchain interactions zJ_1 obtained from the magnetic susceptibilities are listed in table 1 and are compared with our results.

There have been several X-band ESR measurements for powder samples of $Y_2Cu_2O_5$. The g-values obtained by these ESR measurements were similar—around $g \sim 2.1$ [10, 14, 17–19]. Genossar *et al* observed the increase of the linewidth below 120 K, and a further huge increase of the linewidth at 20 K indicating a phase transition [17]. However, Ramakrishna and Ong claimed that the resonance field and the linewidth were temperature independent [14]. We performed a submillimetre-wave ESR measurement for a powder sample of $Y_2Cu_2O_5$ previously [20, 21]. As we used a high frequency and high magnetic field, three different anisotropic g-values were obtained from the ESR absorption lines observed at 86 K, reflecting the deformation of CuO_4 units [20]. They were $g_1 = 2.03$, $g_2 = 2.08$ and $g_\parallel = 2.29$. Moreover the frequency–field relationships observed below T_N were different from those of the usual two-sublattice antiferromagnet [20, 21]. The antiferromagnetic resonance (AFMR) modes could be qualitatively explained by our model [21]. However, it is difficult to explain the magnetization measurements consistently with the AFMR modes. But ambiguity remained due to the use of the powder sample. To facilitate more detailed discussion, we performed a submillimetre-wave ESR measurement using single-crystal $Y_2Cu_2O_5$.

The purpose of this paper is to present for the first time results of submillimetre-wave ESR measurements and magnetization measurements in the static magnetic field for single-crystal $Y_2Cu_2O_5$, and analysis of the AFMR modes below T_N using our model, which was used to interpret our previous magnetization measurements [5, 6].

2. Experimental details

The submillimetre-wave ESR measurements for single-crystal $Y_2Cu_2O_5$ were performed using 60, 70, 80, 90, 100, 110, 120, 130, 140 and 300 GHz Gunn oscillators, and 220 GHz band and 370 GHz band backward-travelling-wave tubes using pulsed magnetic fields up to 16 T in the temperature region from 1.8 K to 265 K. The details of our experimental set-ups can be found in [22] and [23]. The magnetization measurements were performed in a static magnetic field up to 15 T using a vibrating-sample magnetometer at 4.2 K. The magnet used in our experiments is the water-cooled magnet WM-5 of Tohoku University.

The single-crystal samples were very tiny needle-like-shaped ones with dimensions of about $3 \times 0.05 \times 0.05$ mm^3, and with the elongated axis corresponding to the b-axis. We

arranged a number of the samples on a piece of polyethylene sheet so as to have coincidence with the *b*-axes. The distinction between the *a*- and *c*-axes is not apparent, so the ESR absorption line and the magnetization curve observed in the case of $\boldsymbol{H}\perp\boldsymbol{b}$ is the mixing of those for $\boldsymbol{H}\|\boldsymbol{a}$ and $\boldsymbol{H}\|\boldsymbol{c}$. We performed the submillimetre-wave ESR study for the Voigt configuration in the case of $\boldsymbol{H}\|\boldsymbol{b}$, while in the case of $\boldsymbol{H}\perp\boldsymbol{b}$ our experiments were performed both for the Faraday and for the Voigt configuration. The details of our experimental set-ups in the Voigt configuration can be found in [24].

3. Results

3.1. Magnetization measurement

The magnetization curves observed in the static magnetic field are shown by the solid lines in figure 1. The magnetization curve for $\boldsymbol{H}\|\boldsymbol{b}$ is consistent with that observed in the pulsed magnetic field [5]. For $\boldsymbol{H}\|\boldsymbol{b}$, the transition fields H_{c1}, H_{c2}, and the saturation fields $\boldsymbol{H}_{s\|b}$ are $H_{c1} = 2.84$ T, $H_{c2} = 4.71$ T and $\boldsymbol{H}_{s\|b} = 7.3$ T respectively. For $\boldsymbol{H}\perp\boldsymbol{b}$, the magnetization increases linearly and saturates at $H_{s\perp b} = 11.0$ T. The saturated magnetizations for $\boldsymbol{H}\|\boldsymbol{b}$ and for $\boldsymbol{H}\perp\boldsymbol{b}$ are $M_{s\|b} = 1.03\mu_B$ and $M_{s\perp b} = 0.89\mu_B$, respectively. The difference in the saturated magnetization between $\boldsymbol{H}\|\boldsymbol{b}$ and $\boldsymbol{H}\perp\boldsymbol{b}$ comes from the anisotropy of the g-values. The ratio of the saturated magnetizations $M_{s\|b}/M_{s\perp b}$ is consistent with that of the g-values, $g_{\|b}/g_{\perp b}$.

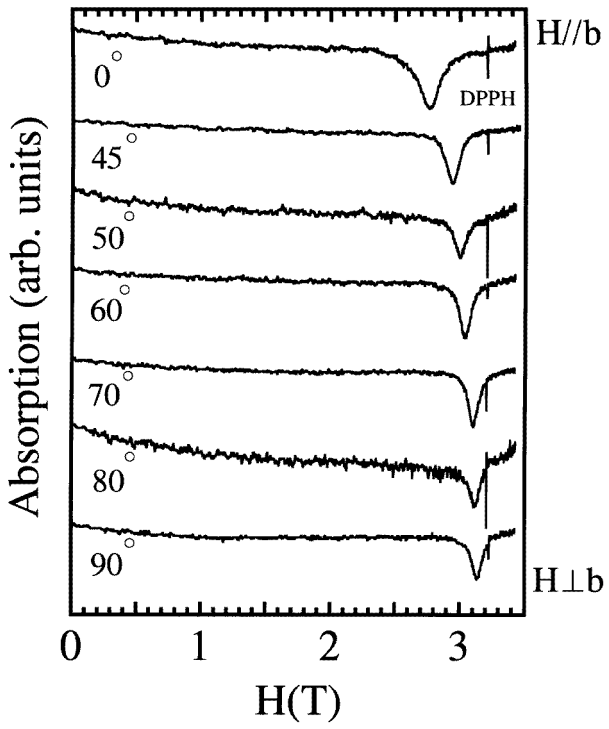

Figure 2. The angular dependence of the EPR absorption line observed at 86 K using 90 GHz.

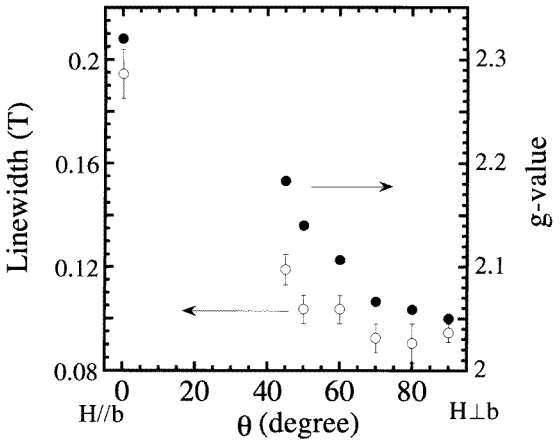

Figure 3. The angular dependence of the linewidth and g-value observed at 86 K using 90 GHz. The linewidth is indicated by open circles and the g-value is indicated by closed circles.

3.2. Electron paramagnetic resonance (EPR)

Figure 2 shows the angular dependence of the EPR absorption line observed at 86 K using 90 GHz. The g-values for $\boldsymbol{H}\|\boldsymbol{b}$ and $\boldsymbol{H}\perp\boldsymbol{b}$ are

$$g_{\|b} = 2.32 \qquad \text{and} \qquad g_{\perp b} = 2.05 \tag{1}$$

respectively. The magnitudes of the g-values are typical of copper oxides. They are consistent with the value $g = 2.1$ for the powder sample obtained from the X-band ESR [10, 14, 17–19] if we assume the average $g = (g_{\|b} + 2g_{\perp b})/3$. Comparing with the results of our submillimetre-wave ESR measurement for the powder sample [20], $g_1 = 2.03$ and $g_2 = 2.08$ seem to correspond to the g-values of the principal direction perpendicular to the b-axis. Despite the mixing of $\boldsymbol{H}\|\boldsymbol{a}$ and $\boldsymbol{H}\|\boldsymbol{c}$, only one absorption is observed for $\boldsymbol{H}\perp\boldsymbol{b}$. This fact may be due to the rather broad linewidth compared with the difference in resonance field between $\boldsymbol{H}\|\boldsymbol{a}$ and $\boldsymbol{H}\|\boldsymbol{c}$. The angular dependence of the linewidth and g-value are shown in figure 3. The linewidth seems to broaden as θ approaches zero.

Figure 4 shows the temperature dependence of the absorption line for $\boldsymbol{H}\|\boldsymbol{b}$ observed at 90 GHz. As the temperature is decreased, the EPR absorption line becomes broader and then vanishes near T_N. Then the new absorption line, which corresponds to AFMR below T_N, appears at the lower magnetic field. The temperature dependence of the linewidth and the resonance field are plotted in figure 5 and figure 6, respectively. The large increase of the linewidth near T_N is consistent with the observation of Genossar *et al* [17].

Figure 7 shows the temperature dependence of the resonance fields observed at 370.4 GHz for $\boldsymbol{H}\|\boldsymbol{b}$ and $\boldsymbol{H}\perp\boldsymbol{b}$. Large EPR shifts above T_N are observed. As the temperature is decreased, the resonance field for $\boldsymbol{H}\|\boldsymbol{b}$ shifts towards the lower field while that for $\boldsymbol{H}\perp\boldsymbol{b}$ shifts towards the higher field. These behaviours are similar to the g-shifts observed for quasi-one-dimensional antiferromagnets [25].

3.3. Antiferromagnetic resonance (AFMR)

Figures 8(a) and 8(b) show the absorption lines of the antiferromagnetic resonance (AFMR) observed at 1.8 K for $\boldsymbol{H}\|\boldsymbol{b}$ and $\boldsymbol{H}\perp\boldsymbol{b}$, respectively. The dotted lines show the critical fields

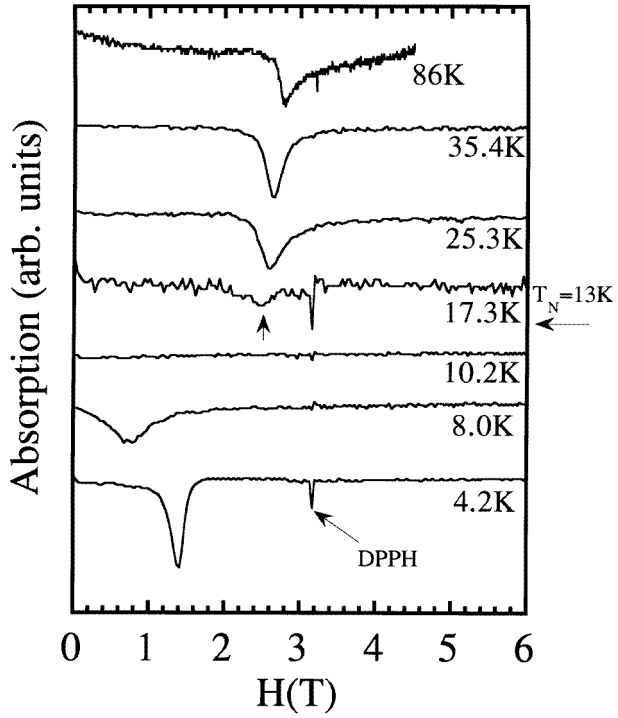

Figure 4. The temperature dependence of the absorption line observed at 90 GHz for $\boldsymbol{H}\|\boldsymbol{b}$.

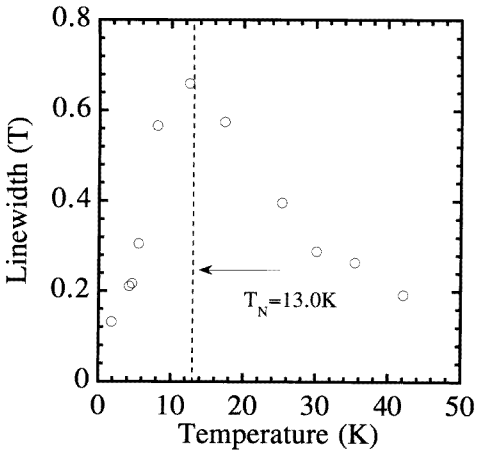

Figure 5. The temperature dependence of the linewidth observed at 90 GHz for $\boldsymbol{H}\|\boldsymbol{b}$.

H_{c1}, H_{c2}, and the saturation fields $H_{s\|b}$, $H_{s\perp b}$ obtained by our magnetization measurement in a static magnetic field. In the case of $\boldsymbol{H}\perp\boldsymbol{b}$ the observed absorption intensities are stronger in the Voigt configuration than in the Faraday configuration. Figure 8(b) shows the case of the Voigt configuration. The absorption lines are observed for all magnetic phases in the case where $\boldsymbol{H}\|\boldsymbol{b}$. The antiferromagnetic resonances in the magnetic phase between H_{c1}

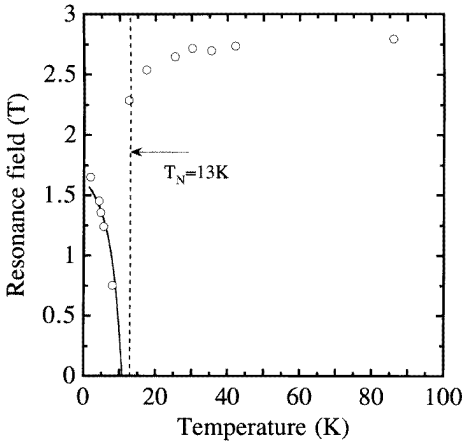

Figure 6. The temperature dependence of the resonance field observed at 90 GHz for $\boldsymbol{H}\|\boldsymbol{b}$. The solid line shows the theoretical curve calculated using our model. See the text for the details.

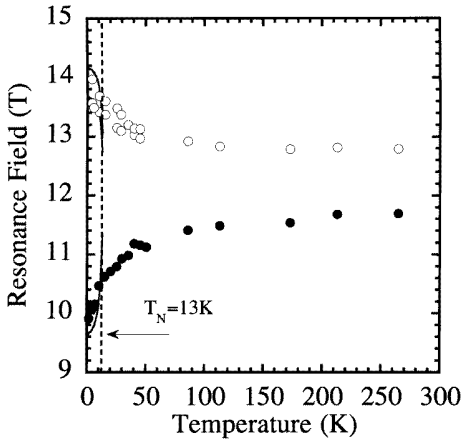

Figure 7. The temperature dependence of the resonance fields observed at 370.4 GHz for $\boldsymbol{H}\|\boldsymbol{b}$ and $\boldsymbol{H}\perp\boldsymbol{b}$.

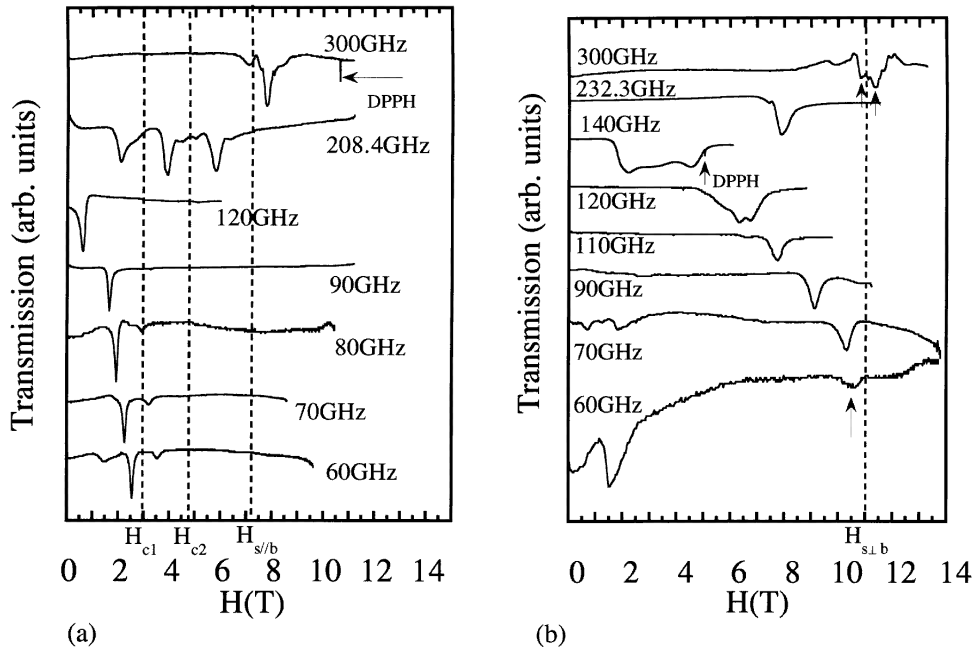

Figure 8. Absorption lines of the antiferromagnetic resonances observed at 1.8 K for $\boldsymbol{H}\|\boldsymbol{b}$ (a) and $\boldsymbol{H}\perp\boldsymbol{b}$ (b). The dashed lines show the transition fields H_{c1}, H_{c2} and the saturation fields $H_{s\|b}$, $H_{s\perp b}$.

and H_{c2} for $\boldsymbol{H}\|\boldsymbol{b}$ are observed in the 220 GHz band and the frequency region just below 80 GHz. Small absorption lines, which may correspond to the critical field resonance, are observed at the vicinity of the critical fields H_{c1} and H_{c2}. There are also strange absorption lines at around 1.5 T below 70 GHz. They cannot be explained by the impurity, because the

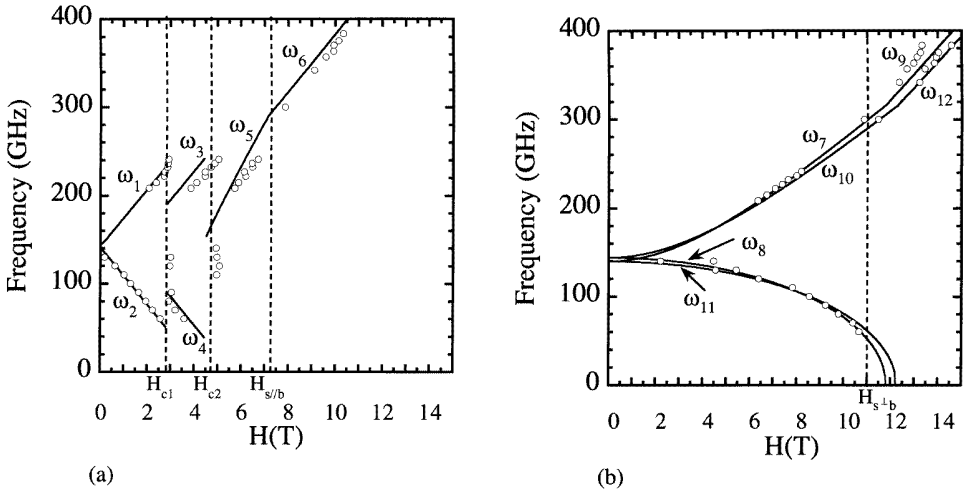

Figure 9. Frequency–field diagrams of the AFMR observed at 1.8 K for $\boldsymbol{H}\|\boldsymbol{b}$ (a) and $\boldsymbol{H}\perp\boldsymbol{b}$ (b). The solid lines correspond to the calculated AFMR modes. See the text for the details.

resonance fields of these absorption lines depend little on the frequency and the direction of the magnetic field. It is not clear at this moment whether these absorption lines are intrinsic or not. The frequency–field relationships for the AFMR for $\boldsymbol{H}\|\boldsymbol{b}$ and $\boldsymbol{H}\perp\boldsymbol{b}$ are shown in figures 9(a) and 9(b) respectively. For $\boldsymbol{H}\|\boldsymbol{b}$, different AFMR modes appear in each magnetic phase, reflecting the magnetic transitions. The AFMR mode observed between H_{c1} and H_{c2} cannot be explained by the conventional two-sublattice model. The analysis of the AFMR modes using our model will be discussed in the next section.

4. Analysis and discussion

The AFMR modes of $Y_2Cu_2O_5$ are now analysed by the conventional molecular-field theory using our model. According to our model, we assume that two Cu^{2+} spins produce a dimer with $S = 1$ and that these dimers are coupled by the antiferromagnetic interactions J_1 and J_2 which correspond to the interchain interaction and the intrachain interaction, respectively [5, 6]. We assume that the main part of the anisotropy comes from the effective single-ion anisotropy induced by the anisotropic exchange interaction within the dimer, and that the interdimer anisotropic exchange interactions are negligibly small because they are estimated to be of the order of $(\Delta g/g)^2 J_{1,2} \sim |J_1/100|$ and $|J_2/100|$, respectively. Proposed magnetic structures when an external field is applied to the b-axis are shown in figure 10. We assume that the antiferromagnetic structure below H_{c1}, which is determined by the neutron diffraction measurements [9, 10], changes to a ferrimagnetic structure between H_{c1} and H_{c2} and then to a spin-flop structure or a helical structure between H_{c2} and $H_{s\|b}$. Which magnetic structure is stable between H_{c2} and $H_{s\|b}$ is determined from the ratio $|J_2/J_1|$. In the case where $|J_2/J_1| < 0.5$ the spin-flop structure should be realized, while in the case where $|J_2/J_1| > 0.5$ the helical structure should be realized in this magnetic phase. Finally the ferromagnetic structure is realized above the saturation field $H_{s\|b}$. As shown in figure 10(b), the ferrimagnetic structure which is assumed in the magnetic phase between H_{c1} and H_{c2}, is described by six sublattices. Therefore the free energy of this system should be

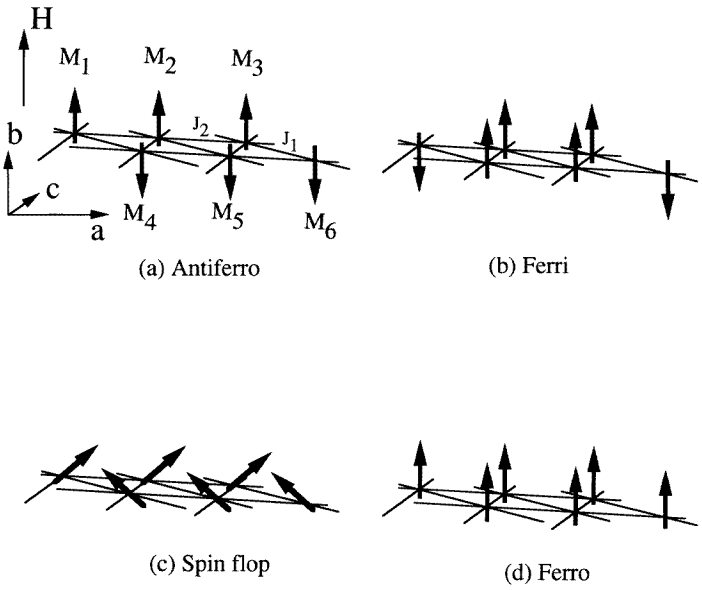

Figure 10. Proposed magnetic structures when the magnetic field is applied to the *b*-axis; (a), (b), (c) and (d) correspond to antiferromagnetic, ferrimagnetic, spin-flop and ferromagnetic structures, respectively. The arrows correspond to the magnetic moments of the dimers with $S = 1$. The magnetic moments are pointing parallel or opposite to the *b*-axis except for in the case of (c). In the case of (c), the magnetic moments lie in the plane containing the *b*-axis. We cannot determine whether the magnetic moments lie in the *ab*-plane or the *bc*-plane, because no distinction between the *a*- and *c*-axes is apparent.

expressed by the six-sublattice model as follows:

$$\begin{aligned} F = {} & A_1(\boldsymbol{M}_1 \cdot \boldsymbol{M}_6 + \boldsymbol{M}_1 \cdot \boldsymbol{M}_4 + \boldsymbol{M}_2 \cdot \boldsymbol{M}_4 + \boldsymbol{M}_2 \cdot \boldsymbol{M}_5 + \boldsymbol{M}_3 \cdot \boldsymbol{M}_5 + \boldsymbol{M}_3 \cdot \boldsymbol{M}_6) \\ & + A_2(\boldsymbol{M}_1 \cdot \boldsymbol{M}_2 + \boldsymbol{M}_2 \cdot \boldsymbol{M}_3 + \boldsymbol{M}_3 \cdot \boldsymbol{M}_1 + \boldsymbol{M}_4 \cdot \boldsymbol{M}_5 \\ & + \boldsymbol{M}_5 \cdot \boldsymbol{M}_6 + \boldsymbol{M}_6 \cdot \boldsymbol{M}_4) + \tfrac{1}{2} \sum_i \boldsymbol{M}_i \Gamma' \boldsymbol{M}_i - \sum_i \boldsymbol{M}_i H \end{aligned} \tag{2}$$

where $\boldsymbol{M}_i$ is ith-sublattice moment. The first and the second term represent the interchain interaction J_1 and intrachain interaction J_2. The coefficients A_1 and A_2 are given by

$$A_1 = -\frac{6}{N}\frac{4J_1}{(g\mu_B)^2} \qquad A_2 = -\frac{6}{N}\frac{2J_2}{(g\mu_B)^2}. \tag{3}$$

The third term represents the anisotropy with the tensor form expressed as follows:

$$G = \begin{pmatrix} \Gamma'_x & & \\ & \Gamma'_y & \\ & & \Gamma'_z \end{pmatrix} \tag{4}$$

where

$$\Gamma'_x + \Gamma'_y + \Gamma'_z = 0. \tag{5}$$

We define the x-, y-, z-axes to be the easy axis, the second easy axis and the hard axis, respectively. We choose the g-values as $g_{\|b} = 2.32$ for $\boldsymbol{H} \|$ easy axis, $g_2 = 2.08$ for $\boldsymbol{H} \|$ second easy axis, and $g_1 = 2.03$ for $\boldsymbol{H} \|$ hard axis, respectively. According to the method used in the case of $NiCl_2{\cdot}2H_2O$ [7], the resonance conditions and the transition

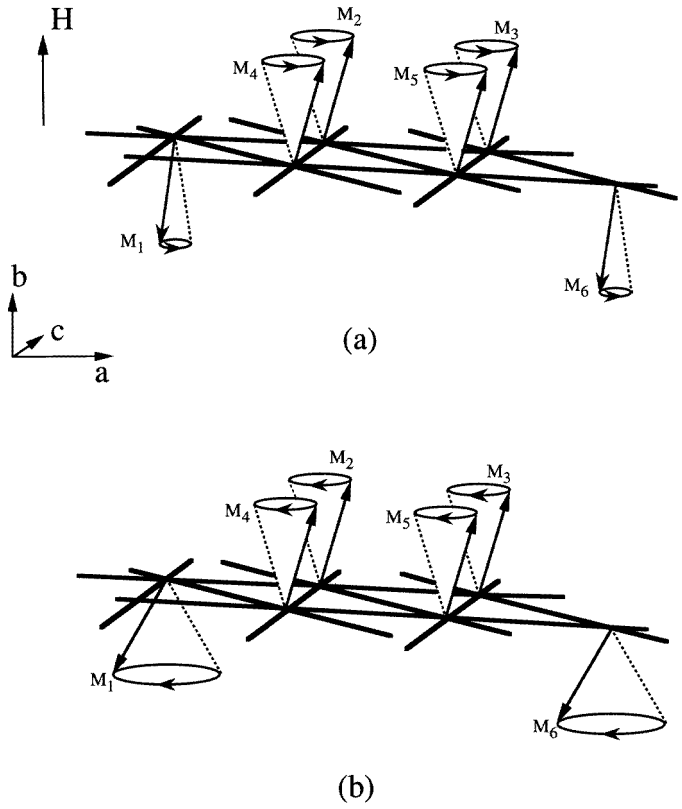

Figure 11. The motions of the sublattice moments of the ESR modes calculated for the magnetic phase $H_{c1} < H < H_{c2}$. (a) and (b) correspond to the high-frequency mode ω_3 and the low-frequency mode ω_4, respectively.

fields for $Y_2Cu_2O_5$ were already calculated and presented in [21]. We will use the same notation as in [21] for the resonance modes as shown in figures 9(a) and 9(b). The ESR modes $\omega_1, \omega_2, \omega_5, \omega_6, \omega_7, \omega_8, \omega_9, \omega_{10}, \omega_{11}$ and ω_{12} calculated for the magnetic phases $0 < H < H_{c1}, H_{c2} < H < H_{s\|b}$ and $H_{s\|b} < H$ for $\boldsymbol{H}\|\boldsymbol{b}$ and for $\boldsymbol{H}\perp\boldsymbol{b}$ are the same as those of the usual two-sublattice antiferromagnet, because the magnetic structures in those magnetic phases are described by the two-sublattice model. In those cases, the sublattice moments $\boldsymbol{M}_1, \boldsymbol{M}_2$ and $\boldsymbol{M}_3$ or $\boldsymbol{M}_4, \boldsymbol{M}_5$ and $\boldsymbol{M}_6$ have the same phases. The motions of the sublattice moments of these ESR modes can be found in [26]. For the magnetic phase $H_{c1} < H < H_{c2}$ whose magnetic structure is described by the six-sublattice model, six ESR modes can be obtained. However, not all of the ESR modes are observable, because the modes are observable only when the total magnetization is in motion. As a result, only two ESR modes are observable. The motions of the sublattice moments of the observable ESR modes are shown in figures 11(a) and 11(b). Figures 11(a) and 11(b) correspond to the ω_3- and ω_4-modes, respectively. In both cases, $\boldsymbol{M}_1$ and $\boldsymbol{M}_6$ or $\boldsymbol{M}_2, \boldsymbol{M}_3, \boldsymbol{M}_4$ and $\boldsymbol{M}_5$ have the same phases. The phase difference between $\boldsymbol{M}_1$ and $\boldsymbol{M}_2$ is π. The ω_3- and ω_4-modes precess in opposite directions as shown in figure 11.

There are four unknown parameters, i.e. the exchange fields H_{E1}, H_{E2}, which correspond to interchain interaction J_1 and intrachain interaction J_2, respectively, and the orthorhombic

anisotropy fields H_{A1}, H_{A2}. They can be expressed as follows:

$$\begin{aligned} H_{E1} &= 2A_1M_0 & H_{E2} &= 2A_2M_0 \\ H_{A1} &= (\Gamma'_y - \Gamma'_x)M_0 & H_{A2} &= (\Gamma'_z - \Gamma'_x)M_0. \end{aligned} \tag{6}$$

Here M_0 is the magnetization of sublattice moment given by

$$M_0 = \frac{1}{6}Ng\mu_B S \tag{7}$$

where S is the spin of the dimer with $S = 1$. From the neutron diffraction measurement, the magnetic moment of a copper ion is estimated to be $1.06\mu_B$ per ion [9]. Therefore we assume the magnetic moment of the dimer $g\mu_B S$ to be $2.12\mu_B$. The parameters H_{E1}, H_{E2}, H_{A1} and H_{A2} are determined by applying the calculated results to the experimental results on zero-field resonance frequencies, the AFMR modes above $H_{s\|b}$ for $\boldsymbol{H}\|\boldsymbol{b}$ and the first transition field H_{c1}. They are as follows:

$$\begin{aligned} H_{E1} &= 5.15\ \text{T} & H_{E2} &= 0.93\ \text{T} \\ H_{A1} &= 2.0\ \text{T} & H_{A2} &= 2.1\ \text{T}. \end{aligned} \tag{8}$$

As the ratio H_{E2}/H_{E1} turned out to be 0.2, the spin-flop structure is more stable in the phase between H_{c2} and $H_{s\|b}$ than the helical structure, in contrast to the case for $NiCl_2{\cdot}2H_2O$ where the magnetic structure in this phase is considered to be the helical structure [7]. The calculated transition fields are obtained as follows:

$$\begin{aligned} H_{c1} &= 2.84\ \text{T} & H_{c2} &= 4.51\ \text{T} & H_{s\|b} &= 7.2\ \text{T} \\ H_{s\perp b1} &= 11.8\ \text{T} & H_{s\perp b2} &= 12.3\ \text{T} \end{aligned} \tag{9}$$

where $H_{s\perp b1}$ and $H_{s\perp b2}$ are the saturation field for the second easy axis and the hard axis, respectively. The theoretical curves for AFMR modes obtained from our model are shown by the solid lines in figures 9(a) and 9(b). It turned out that all of the AFMR modes expected from our model are observed. The crystalline-field constants of the effective single-ion-type anisotropies D and E are estimated from the following relations [27]:

$$\begin{aligned} D &= -\frac{g\mu_B S(H_{A1} + H_{A2})}{S(S - \frac{1}{2})} \\ E &= \frac{g\mu_B S(H_{A2} - H_{A1})}{S(S - \frac{1}{2})}. \end{aligned} \tag{10}$$

D and E are calculated as

$$D = -3.35\ \text{K} \qquad \text{and} \qquad E = 0.08\ \text{K}. \tag{11}$$

The intradimer exchange interaction J_0 is roughly estimated to be 340 K from the following relation:

$$|D| \sim (\Delta g/2)^2 J_0. \tag{12}$$

We consider this magnitude of J_0 to be reasonable in the case of copper oxides. From H_{E1} and H_{E2}, both interdimer exchange interactions J_1 and J_2 are estimated to be antiferromagnetic. The magnitudes of J_1 and J_2 are calculated as

$$J_1 = -0.92\ \text{K} \qquad \text{and} \qquad J_2 = -0.33\ \text{K}. \tag{13}$$

Although the intrachain interaction J_2 is evaluated as antiferromagnetic, the ferromagnetic arrangement of Cu^{2+} spins in the chain in zero magnetic field can be realized because the magnitude of the interchain interaction J_1 is estimated to be larger than that of J_2. The ratios $|J_1/J_0|$ and $|J_2/J_0|$ are estimated to be of the order of 1/380 and 1/1100, respectively.

The intrachain interactions J_0, J_2 and the sums of the interchain interactions zJ_1 obtained from our analysis are shown in table 1. In our case $z = 4$. The sums of the interchain interactions zJ_1 obtained from our analysis seem to be comparable with that obtained by Ramakrishna and Ong [14] and Janicki and Troc [15] from the magnetic susceptibility using the quasi-one-dimensional chain model. However, the intradimer interaction J_0 is rather large compared with that obtained from the magnetic susceptibility [14–16]. It is clear that the quasi-one-dimensional chain model cannot explain the existence of the metamagnetic transition, because the ratio $|J_2/J_0|$ estimated by Paillaud *et al* [16] is 1/1.23. The dimer with $S = 1$ cannot be produced by their model.

The temperature dependence of the resonance field below T_N can be calculated by considering the temperature dependence of the magnitude of the sublattice moment M_0 which is obtained from the neutron diffraction measurement [9]. The calculated result shows good agreement with the experimental result observed at 90 GHz for $\boldsymbol{H} \| \boldsymbol{b}$ as shown by the solid line in figure 6. The experimental results observed at 370.4 GHz are also explained by same analysis except for near T_N, as shown by the solid lines in figure 7. According to this analysis, the resonance field should be constant above T_N because the sublattice moment M_0 is zero. However, a continuous shift of the resonance fields from the paramagnetic state to the antiferromagnetic state is observed at 370.4 GHz.

From the above analysis, the AFMR of $Y_2Cu_2O_5$ can be explained by our model fairly well, except the small discrepancies in the phase between H_{c1} and H_{c2} and between H_{c2} and $H_{s\|b}$ for $\boldsymbol{H} \| \boldsymbol{b}$. However, there exist some other discrepancies between the experimental results and calculated results. Our model is not consistent with the large EPR shifts observed above T_N, because the results of the analysis indicate that the interchain interaction J_1 is comparable to the intrachain interaction J_2, which indicates that there exist three-dimensional exchange interactions in this material. Moreover the magnetization curve in the magnetic phase between H_{c2} and $H_{s\|b}$ cannot be explained by the molecular-field theory. The magnetization $M(H)$ can be calculated from the following relation:

$$M(H) = \frac{\partial F}{\partial H}. \tag{14}$$

The theoretical magnetization curve which is calculated with the parameters obtained from the analysis of the AFMR is shown by the dashed line in figure 1. The theoretical magnetization curve between H_{c2} and $H_{s\|b}$ is calculated as follows:

$$M(H) = \frac{M_s H}{2H_{E1} - H_{A1}} \tag{15}$$

where M_s is the saturated magnetization. Therefore if the spin-flop structure is realized in this magnetic phase as assumed in our model, the extrapolation of the linear magnetization must cross the origin. However, the extrapolation of the experimental result does not cross the origin. This fact suggests that the magnetic phase between H_{c2} and $H_{s\|b}$ cannot be interpreted by the molecular-field theory.

5. Conclusion

Submillimetre-wave ESR measurements for the single-crystal $Y_2Cu_2O_5$ have been performed for the first time. The AFMR modes were explained using our model which is essentially a molecular-field theory. However, large EPR shifts, which are similar to those of the one-dimensional antiferromagnet, are observed above T_N. These shifts are not consistent with our model, because the analysis using our model suggests that there exist three-dimensional exchange interactions in this material. Moreover the magnetic phase

between H_{c2} and $H_{s\|b}$ cannot be interpreted with molecular-field theory. In order to clarify the magnetic structure in the magnetic phase between H_{c2} and $H_{s\|b}$, a neutron diffraction experiment under a magnetic field up to $H_{s\|b}$ is required.

Acknowledgments

The authors SK and HO are grateful to Professor T Nanba of Kobe University for his encouragement and support. The authors are also grateful to Professor K Nagasaka of the Science University of Tokyo for supplying the InSb detector. The authors wish to thank the staff of the High-field Laboratory and Cryogenic Centre, Tohoku University, for operating the magnet. This work was partly supported by a Grant-in-Aid for Scientific Research from the Ministry of Education, Science and Culture.

References

[1] Troc R, Bukowski Z, Horyn R and Klamut J 1987 *Phys. Lett.* **125A** 222
[2] Moshchalkov V V, Samarin N A, Grishchenko I O, Mill B V and Zoubkova Y 1990 *J. Magn. Magn. Mater.* **90+91** 533
[3] Cheong S-W, Thompson J D, Fisk Z, Kubat-Martin K A and Garcia E 1988 *Phys. Rev.* B **38** 7013
[4] Jang W-J, Hasegawa M, Zhao T R, Takei F, Tamura M and Kinoshita M 1994 *J. Cryst. Growth* **141** 153
[5] Motokawa M, Kita K, Shibazaki H, Ohta H, Jang W-J, Hasegawa M and Takei H 1995 *Physica* B **211** 165
[6] Ushiroyama H, Kita K, Kimura S, Ohta H and Motokawa M 1994 *Physica* B **201** 95
[7] Motokawa M 1970 *Proc. 12th Int. Conf. on Low Temperature Physics (Kyoto)* (Tokyo: Keigaku) p 703
[8] Freund H R and Muller-Buschbaum H 1977 *Z. Naturf.* b **32** 609
[9] Garcia-Munoz J L, Rodriguez-Carvajal J, Obradors X, Vallet-Regi M, Gonzalez-Calvet J and Garcia E 1990 *Phys. Lett.* **149A** 319
[10] Aride J, Flandrois S, Taibi M, Boukhari A, Drillon M and Soubeyroux J L 1989 *Solid State Commun.* **72** 459
[11] Kazei Z A, Kolmakova N P, Levitin R Z, Mill B V, Moshchalkov V V, Orlov V N, Snegrev V V and Zoubkova Ja 1990 *J. Magn. Magn. Mater.* **86** 124
[12] Garcia-Munoz J L, Rodriguez-Carvajal J, Obradors X, Vallet-Regi M, Gonzalez-Calvet J and Parras M 1991 *Phys. Rev.* B **44** 4716
[13] Motokawa M 1973 *J. Phys. Soc. Japan* **35** 315
[14] Ramakrishna B L and Ong E W 1988 *Solid State Commun.* **68** 775
[15] Janicki J and Troc R 1992 *J. Phys.: Condens. Matter* **4** 6267
[16] Paillaud J L, Legoll P and Drillon M 1991 *J. Magn. Magn. Mater.* **96** 41
[17] Genossar J, Shaltiel D, Zevin V, Grayevsky A and Fisher B 1989 *J. Phys.: Condens. Matter* **1** 9471
[18] Ganguly P, Sreedhar K, Raju A R, Demazeau G and Hagenmuller P 1989 *J. Phys.: Condens. Matter* **1** 213
[19] Bowden G L, Elliston P R, Wen K T, Dou S X, Esterling K E, Bourdillon A, Sorrell C C, Cornell B A and Separovic F 1987 *J. Phys. C: Solid State Phys.* **20** L545
[20] Kimura S, Kaneko K, Ohta H and Motokawa M 1994 *Physica* B **201** 115
[21] Kimura S, Ohta H and Motokawa M 1996 *J. Phys. Soc. Japan* **65** 297
[22] Motokawa M, Ohta H and Makita N 1991 *Int. J. Infrared Millimeter Waves* **12** 149
[23] Ohta H, Yoshida K, Matsuya T, Nanba T, Motakawa M, Yamada K, Endoh Y and Hosoya S 1992 *J. Phys. Soc. Japan* **61** 2921
[24] Ohta H, Imagawa S, Motokawa M and Kita E 1993 *J. Phys. Soc. Japan* **62** 4467
[25] Nagata K and Tazuke Y 1972 *J. Phys. Soc. Japan* **32** 337
[26] Foner S 1963 *Magnetism I* ed G T Rado and H Suhl (New York: Academic) p 383
[27] Kanamori J and Minatono H 1962 *J. Phys. Soc. Japan* **17** 1759